Journal of Imaging Science and Technology® 66(4): 040417-1–040417-9, 2022.
© Society for Imaging Science and Technology 2022

Accurate Power Modelling Framework for Medical Images in Embedded System

Kai Liu
College of Educational Science, Qiannan Normal University for Nationalities, Duyun, 558000, Guizhou, China

Junke Li
College of Educational Science, Qiannan Normal University for Nationalities, Duyun, 558000, Guizhou, China
School of Computer and Information, Qiannan Normal University for Nationalities, Duyun, 558000, Guizhou, China
Key Laboratory of Machine learning and Unstructured Data Processing of Qiannan, Duyun 558000, Guizhou, China
E-mail: junker_li@sgmtu.edu.cn

Jincheng Zhou and Mingjiang Li
School of Computer and Information, Qiannan Normal University for Nationalities, Duyun, 558000, Guizhou, China
Key Laboratory of Complex Systems and Intelligent Optimization of Guizhou, Duyun 558000, Guizhou, China

Abstract. *The display in embedded devices is a significant energy-consuming device, and the display content determines the degree of energy consumption. In the practice of energy saving and emission reduction, it is necessary to build an accurate medical image power prediction model for the display. Current power consumption prediction models for medical images often focus on the performance of a single prediction model, ignoring the ability of multiple single prediction models to improve performance. This paper proposes an accurate medical power framework (AMPF), which consists of three steps. In the first step, the strong predictor is used to compose multiple RGB single channels to obtain the power model. In the second step, the power between RGB channels is represented by errors, and the power generated by RGB channel dependence is obtained by the strong predictor method. The third step is to compose the power of the first step and the second step to get accurate medical image power prediction results. The experimental results show that the accuracy of the AMFP proposed in this paper reaches 0.9798, which is 6.836% higher than that of the single power model. The AMPF implemented by AdaBoost is superior to that implemented by EWM in performance and has about 1.3 times the time advantage in training.* © *2022 Society for Imaging Science and Technology.*
[DOI: 10.2352/J.ImagingSci.Technol.2022.66.4.040417]

1. INTRODUCTION

The objects of medical image processing are medical images with different imaging mechanisms. The types of medical imaging widely used in clinics mainly include X-CT (X-ray imaging), MRI (magnetic resonance imaging), NMI (nuclear medical imaging) and UI (ultrasonic imaging). In the current imaging medical diagnosis, it is mainly to find the diseased body segment by observing a group of two-dimensional slice images, which often relies on doctors' experience. Using the computer image processing technology to analyze and process the two-dimensional slice image can realize the segmentation, extraction, three-dimensional reconstruction, and three-dimensional display of human organs, soft tissue, and diseased body. These can assist doctors in qualitative or even quantitative analysis of the diseased body segment and other relevant areas, to greatly improve the accuracy and reliability of medical diagnosis. It can also play an important auxiliary role in medical teaching, surgical planning, surgical simulation, and various medical research [1–4].

On the other hand, with the development of the ICT industry, we have entered a new industrial era represented by the intelligent mobile terminal, intelligent wear equipment, virtual reality, intelligent robot, and the internet of things, which makes embedded computing gradually become the mainstream. Taking a typical embedded device smart mobile terminal as an example, the power consumption of the display screen usually accounts for 27–50% of the whole system power [5–8]. Although the power consumption of a single device is not high (the average power consumption is 0.3w–1W), the global holdings of smartphones have already exceeded 2.3 billion. Due to the wide variety, wide application range, and the huge number of embedded devices, the overall power consumption is crucial, especially for intelligent mobile terminals, intelligent wearable devices, and virtual reality devices with limited battery capacity. Reducing display power, improving device life, and prolonging service life has become an important issue.

At present, the most representative display technology is the OLED screen, which uses a thin organic material coating and glass substrate. When a device is powered on, it drives the organic material to emit light and produce different colors. Each pixel of an OLED screen is composed of three kinds of sub pixels: Red, Green and Blue. Due to the self-luminous characteristics of OLED, the luminescence of each sub-pixel can be controlled independently. Therefore, the image power of an OLED screen is completely determined by the display

Received Jan. 15, 2022; accepted for publication June 12, 2022; published online June 29, 2022. Associate Editor: Hamad Hamad Naeem.
1062-3701/2022/66(4)/040417/9/$25.00

content, more specifically, the pixel values of all pixels in the content [9, 10].

Since medical instruments and equipment are typically embedded equipment, the power modeling of their display images is helpful for medical image task scheduling, medical image analysis, prolonging the service life of the equipment, and improving the display effect. Considerable work has been done to study them [11–24]. Although the current power model can acquire the medical image's power, there is the issue of low accuracy [17, 20, 22, 24]. To solve this problem, this paper proposes an accurate medical power framework (AMPF) by using a strong prediction method composed of multiple single predictors and a regression approach. The experimental results demonstrate that the AMPF model has higher accuracy than the single prediction model. Thus, our contributions of this paper are:

(1) We summarize the current power models of medical images and analyze the shortcomings of current research.
(2) To overcome the shortcomings, we propose an AMPF framework, which first obtains the power of RGB independent channels, then obtains the power of RGB channel interdependence, and finally combines them to obtain more accurate power value.
(3) We verify the feasibility and effectiveness of the AMPF framework, and the results show that the AMPF framework is effective and has high accuracy.

2. RELATED WORK

Power modeling is the basis of computing power and low power scheduling, and it is also the main quantitative index to evaluate the effect of power optimization. At present, the power modeling of the image on an OLED screen is mainly divided into two types: the power consumption statistical model based on hardware sensors and the approximate estimated power consumption model based on software. The former mainly measures the power through the power consumption measuring instrument or counts the power consumption through the access circuit embedded in the OLED display component through the hardware sensor. The latter is to calculate the power by establishing the power model of an OLED screen. The measurement results based on hardware are usually more accurate than those based on software estimation, but special hardware is required for measurement. The approximate estimation method based on software calculates the power consumption by constructing the power consumption model, which is simple and universal. At present, the power modeling method based on software approximate estimation has become the consensus of researchers at home and globally [5–24].

In energy-saving modeling, Hort et al. [11] showed that the research on OLED power is an important research direction for embedded systems. Duan et al. [12] presented a low-energy OLED method on HSV color space by integrating brightness adjustment and saturation adjustment to decrease the display power of images. Li et al. [13] extracted the display content through the visual saliency algorithm, and then dynamically adjusted the pixels of each region based on visual attention to reducing energy. Asnani et al. [14] generated energy-saving and contrast-enhanced images by using the image-related power quality of OLED displays, and achieved the goal of reducing image power consumption by reducing the RGB intensity level in color images. Dalton et al. [15] used the webcam installed on the laptop monitor to regularly capture images, and then determined whether the user was watching the monitor according to the face detection algorithm to enhance the power management. Na et al. [16] believed that the degradation of image quality was caused by delayed saturation voltage. By reducing OLED charging delay to eliminate image degradation, they explored a new way to obtain excellent image quality under ultra-low brightness. Zhou et al. [17] have shown that the high luminous efficiency and top-emitting structure of OLEDs can greatly reduce power consumption.

In the software based power model, the power model is constructed according to the imaging process. In a typical intelligent mobile terminal system, the operating system and application software run on the main processor, and the graphics processing unit (usually including the graphics accelerator and display controller) generates the bitmap of the display content and then stores it in the frame buffer memory. Then, the bitmap is sent to the display for showing. According to this process, the software-based OLED display power model can be divided into code level power model [15, 19, 21], image-level power model [13, 14, 19], circuit-level power model [16–18, 20] and pixel-level power model [13, 19, 22–24]. Lim et al. [18] considered that the existing display power supply model did not take the impact of I-R voltage drop into consideration. Therefore, the AMOLED display power model was proposed by using the method of compensating I-R voltage drop. Dong et al. [19] pointed out that when the display shows different colors, it will consume different energy. Then, they provided power model to estimate power based on pixels, images, and codes respectively. Park et al. [20] considered the energy consumption generated by the driving circuit of the display components and their interdependence and then proposed a power model. Kim et al. [21] proposed a runtime power estimation method for OLED displays by monitoring the kernel activities of applications to capture screen change events of running applications. Kim et al. [22] used multiple regression techniques to explain the dependence between R, G, and B channels and proposed a new high-precision and fast power model for AMOLED display. Hong et al. [23] considered the dependence among red, green, and blue (RGB) channels and proposed a new accurate power model. Dash et al. [24] pointed out that the previous OLED power model based on linear regression could not capture the unique behavior of OLED display with large color space and presented a segmented power model by considering linear regression in each small area of huge color space.

Code-level power modeling is usually realized by using high-level language with the help of the user interface, and the interface power is estimated by traversing the types and

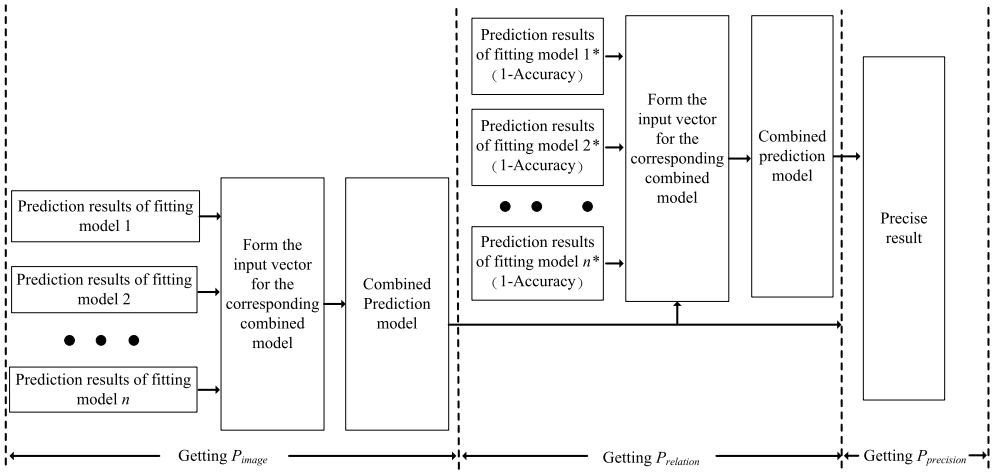

Figure 1. The structure of AMPF.

structure of internal controls. Code-level power modeling depends on the analysis of high-level programming language, and can not calculate the power consumption of natural images. Image level power modeling mainly estimates the current display power by accessing the local bitmap information of the image. Although its calculation speed is fast, the accuracy is not enough. Circuit level power modeling mainly obtains the carrier mobility of thin-film transistor, OLED luminous efficiency, pixel aspect ratio, and other parameters for power calculation. The accuracy of circuit-level power modeling is high, but the generality is not enough. Pixel-level power modeling mainly calculates the current display power by traversing all pixel information of the image. It calculates the display power through image bitmap information. It has high accuracy and strong universality. At present, it is the main method of OLED power modeling. In the pixel-level power model, the model in Dong et al. [19] is widely used. Eq. (1) is its specific power model, where, $f(\cdot)$, $h(\cdot)$, and $k(\cdot)$ represent the power functions of the red, green and blue color components of the pixel respectively. P_{pixel} represents the power consumption of a single pixel, n represents the total number of pixels in the image, C represents the static power of OLED without pixel constraints, and P_{image} represents the power of the whole image. To establish the model, the C parameter can be obtained by measuring a completely black screen. The power function of three color components can be obtained by gradually changing the color intensity when filling the screen with a single color. Using this method, the power of the image can be obtained, but it has few errors [20, 22, 23]. This phenomenon was described in Ref. [20], which pointed out that the reason for the error was that the interdependence between pixels was not considered, and a circuit level power consumption model was proposed to solve it. Based on [20], by further considering the interdependence of R, G, and B channels, [22, 23] use multiple region algorithm to estimate the dependency parameters and build the power model. Summarizing the above references, we believe that the prediction accuracy can be improved by minimizing the difference between the measured results and the results obtained by multiple prediction models. Therefore, using the above ideas, we propose an AMFP (accurate medical power framework) framework to solve the errors caused by the dependency between pixels and improve the prediction accuracy. Section 3 discusses the specific ideas about this method.

$$\begin{aligned} P_{\text{pixel}}(R, G, B) &= f(R) + h(G) + k(B) \\ P_{\text{image}} &= C + \sum_{i=1}^{n} \left\{ f(R_i) + h(G_i) + k(B_i) \right\} \end{aligned} \tag{1}$$

3. OUR PROPOSED AMPF FRAMEWORK

Analyzing the current research studies, considering the energy consumption caused by the relationship between pixels can improve the prediction effect. Therefore, the power model can be expressed by Eq. (2) where, P_{accurate} represent the accurate prediction power of the image, and P_{image} represents the independent power of three-channel, and $P_{\text{relation(R,G,B)}}$ indicates the power generated by the three channel interdependence (including the pairwise relationship between channels and the relationship between three channels). At present, P_{image} has conducted a lot of research studies based on regression methods. According to Eq. (2), to improve the accuracy, the most important thing is to improve the accuracy of $P_{\text{relation(R,G,B)}}$. Therefore, we use Eq. (2) to obtain a more accurate $P_{\text{relation(R,G,B)}}$ by subtracting the power obtained from multiple single regression models from the actual power consumption, and proposes an AMPF framework. Its structure is shown in Figure 1.

$$P_{\text{accurate}} = P_{\text{image}} + P_{\text{relation(R,G,B)}} \tag{2}$$

In Fig. 1, AMPF consists of three parts: Getting P_{image}, getting P_{relation}, and getting P_{accurate}. Among them, getting P_{image}, getting P_{relation}, and getting P_{accurate} respectively corresponds to P_{image}, P_{relation}, and P_{accurate} in Eq. (2).

1. $Indicator(1,:)=ones(1,m)/m;$
2. $for\ \ i=1:k$
3. $\quad Count(i)=0$
4. $\quad for\ \ j=1:m$
5. $\quad\quad if\ \ abs(error_{i,j})>threshold$
6. $\quad\quad\quad Count(i)=Count(i)+P\_Weight(i,j)$
7. $\quad\quad\quad P\_Weight(i+1,j)=P\_Weight(i,j)*number$
8. $\quad\quad else$
9. $\quad\quad\quad P\_Weight(i+1,j)=P\_Weight(i,j)$
10. $\quad\quad end$
11. $\quad end$
12. $w(i)=0.5/\exp(\text{abs}(Count(i)))$
13. $P\_Weight(i+1,:)=P\_Weight(i+1,:)/sum(P\_Weight(i+1,:))$
14. end
15. $w(1)=w(1)/sum(w);w(2)=w(2)/sum(w);...;w(k)=w(k)/sum(w);$

Figure 2. Procedure of AdaBoost.

In getting P_{image}, for overcoming the problem of large power error caused by a single power model, we use the method of combining weak predictors to generate strong predictors. Weak predictors can be non-linear regression model (NLR), support vector machine method (SVM), or neural network method (BP, GRNN, RBF, etc.). The strong predictor can be the entropy weight method (EWM), AdaBoost method, etc. The input of the strong predictor method can be the output of each weak predictor or the error of each weak predictor. In this paper, the error is used as the input of the EWM and AdaBoost strong predictor.

We assume that the number of CT images in training set is $n1$ and the number of CT images in test set is $n2$; $\{M_k|0 <= k < n1\}$ are the gray level in each CT image, $\{\overline{m}_k\}$ are the normalized series corresponding M_k. Using the AMPF realized by EWM for getting the P_{image}, following steps are used.

Step 1. Establishing the single predictor. We use k number of single predictor named the NLR, SVR model, BP, GRN and RBF to train, we can get $\hat{y}_{pr}$, $\hat{y}_{SVR}$, $\hat{y}_{BP}$, $\hat{y}_{GRNN}$ and $\hat{y}_{RBF}$.

Step 2. Getting error data. We then calculate the error of predicted model NLR, SVR, BP, GRNN and RBF as error^m_{NLR}, error^m_{SVR}, error^m_{BP}, error^m_{GRNN}, error^m_{RBF} on training sample set n_1.

Step 3. Calculate the evaluation matrix. After step 2, we can get the evaluation matrix $\boldsymbol{E} = \text{error}_{a\times b}$, where a represents the number of single prediction model; b represents the number of CT images. Normalized the evaluation matrix $\boldsymbol{E}$ by row to get the normalized matrix $NE = \boldsymbol{NE}_{a\times b}$.

Step 4. Calculate the information entropy. Use Eq. (3) to get the information entropy for each single predictor. In Eq. (3), b is the number of CT images.

$$H_i = -\frac{1}{\ln b}\sum_{j=1}^{b} NE_{ij}\ln NE_{ij} \tag{3}$$

Step 5. Calculate the weight of each weak predictors. After getting the information entropy, we can use Eq. (4) to get the weight for each predictors. In Eq. (4), k is the number of single predictors.

$$w_i = \frac{1-H_i}{k-\sum_{i=1}^{k} H_i} \tag{4}$$

Then, combined predictor can be expressed as Eq. (5).

$$P_{\text{combined}} = w_1^{\text{combined}} * NLR(m) + w_2^{\text{combined}} * BP(m) + \cdots + w_n^{\text{combined}} * SVR(m) \tag{5}$$

If using the AMPF realized by AdaBoost method for getting the P_{image}, after step 2, the procedure in Figure 2 can be used to get the w in Eq. (5).

In Fig. 2, m is the number in $n1$. *P_Weight* is used to indicate the weight of the training sample. When the prediction error of the training sample is greater than the *threshold*, increase its value so that the next round will pay more attention to it. For example, in line 7, it is multiplied by *number*. *number* is the trend to be concerned with next time, and its value is greater than 1. *Threshold* is the artificially set threshold value. *Count* is used to accumulating the weights of the training samples of the current weak predictor. M is used to indicate the number of training samples. K is used to indicate the number of weak predictions. At the beginning of the procedure, the weight of each training sample is the same, as shown in line 1. $\text{error}_{i,j}$ represents the jth sample prediction error of the ith predictor. As a whole, lines 4 to 10 complete the sum of the weights that all training samples need to pay attention to under the current weak predictor, and update the weights of the next prediction samples. Line 12 realizes the weight calculation under the current weak predictor. Line13 normalizes the next prediction sample weight. Lines 2-14 calculate their respective weights for K weak predictors under m training samples. Line 15 is the calculation of respective weights under K weak predictors. The result obtained by line 15 is the weight corresponding to each weak predictor in Eq. (5).

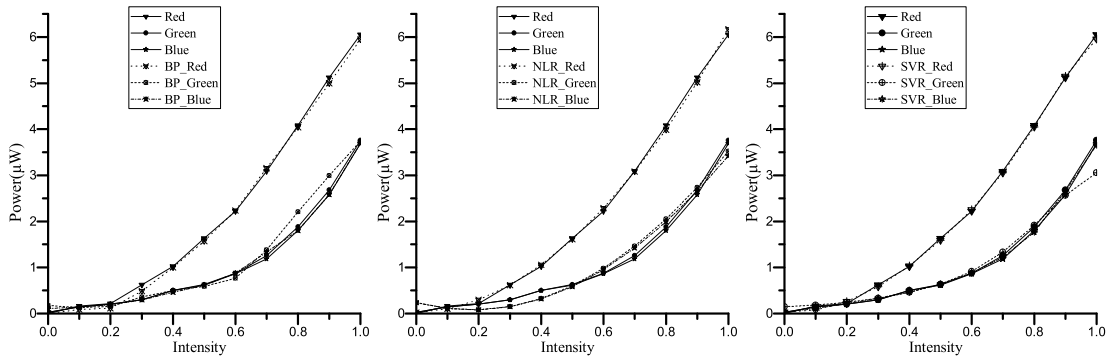

(a) Fitting results of BP method (b) Fitting results of NLR (c) Fitting results of SVR

Figure 3. Curve fitting of three single predictors.

In Getting P_{relation}, the errors of multiple power models are used as the power generated by the three-channel interdependence. In order to obtain reasonable error, we also use the method of combining weak predictors to generate strong predictors. The steps of getting P_{relation} are as follows:

Step 5. We use the accuracy of each model (including the strong predictor model) to represent the error of each model. That is, we use the prediction results multiplied by (1-accuracy) as an error. The calculation of accuracy is shown in Eq. (6), where, *predicted_value* is the output of each weak predictors, and *Actual_value* is the real power value for each image.

$$\text{Accuracy} = \left(\text{predicted\_value}/\text{Actual\_value}\right) * 100\% \quad (6)$$

Step 6. The error of each model was obtained step 5 by subtracting the error of the strong prediction model to obtain the error gap. Input the above gap into the methods of step 3 to step 5 or Fig. 2 to obtain a strong predictor output. This output is the weight for each error obtained by step 5. At this point, P_{relation} can be obtained by Eq. (7).

$$P_{\text{relation}} = w_1^{\text{relation}} * \text{Error}_{NLR(m)} + w_2^{\text{relation}} * \text{Error}_{BP(m)} + \ldots + w_n^{\text{relation}} * \text{Error}_{SVR(m)}. \quad (7)$$

In Getting P_{accurate}, we use Eq. (2) to calculate power obtained in the steps of Getting image and Getting prediction. Finally, an accurate medical image power model is obtained.

4. EXPERIMENT

4.1 *Experimental Platform*

For verifying the proposed CT image power model, The Cancer Imaging Archive (TCIA) [25] is used for testing. The hardware experimental platform of this paper is μOLED-32028-P1 AMOLED with a resolution of 320 × 240, 65K color. Hoiki 3334 multifunctional power measuring instrument is used to measure instantaneous power consumption and cumulative power consumption, and Victor 3005 DC power supply provides stable and controllable voltage. The configuration of the hardware and software platform is shown in Table I. For better testing the effectiveness of the AMPF proposed in this paper, we first randomly extract the images in ACRIN 6684 and ACRIN 6677 to form a data set, and then divide it into two parts: training set and test set. Their ratio is 3:1.

4.2 *Evaluation Index*

Typically, the root mean square error (RMSE), the mean absolute percentage error (MAPE), (mean absolute error (MAE), square sum error (SSE) and the R^2 are mainly evaluation index. Therefore, we select these indexes to evaluate each model. Eq. (8) shows the calculation method for the above indexes.

$$\begin{aligned}
RMSE &= \sqrt{\frac{1}{N}\sum_{i=1}^{n}\left(y_i-\hat{y}_i\right)^2} \\
MAPE &= \frac{1}{N}\sum_{i=1}^{N}\left|\frac{y_i-\hat{y}_i}{y_i}\right| \times 100\% \\
RRMSE &= \sqrt{\frac{1}{N}\sum_{i=1}^{N}\left(\frac{y_i-\hat{y}_i}{y_i}\right)^2} \\
MAE &= \frac{1}{N}\sum_{i=1}^{N}\left|y_i-\hat{y}_i\right| \\
SSE &= \sum_{i=1}^{N}\left(y_i-\hat{y}_i\right)^2 \\
R^2 &= 1-\frac{\sum_{i=1}^{N}\left(y_i-\hat{y}_i\right)^2}{\sum_{i=1}^{N}\left(y_i-\bar{y}_i\right)^2}
\end{aligned} \quad (8)$$

In Eq. (8), N is the number of predicting medical image; y_i is the actual power of the ith medical image; $\hat{y}_i$ is the predicted power of the ith medical image.

4.3 *Experimental Results*

Figure 3 shows the results of curve fitting using the BP method (shown in figure (a)), NLR method (shown in figure (b)), and SVR method (shown in figure (c)). From the figure,

Table I. Hardware experiment platform and data set.

Type	Category	Configuration
Hardware Platform	Display(AMOLED)	Type: μOLED-32028-P1 Resolution: 320 × 240 Color:65K Size:2.83 inch
	Power meter	Type:HOIKI 3332 Accuracy:±0.1 % rdg Power range:15 mW–30 kW Sampling frequency: 1 Hz–100 kHz Cumulative measurement range: 0–±999999MWh
	Power supply	Type: victor 3005 Voltage Accuracy:0.05 %+3mV Current Accuracy: 0.2 %+5mA Voltage range:0–30V Current range: 0–5A
Image data set	ACRIN 6684	Modalities: CT, MR, PET Number of Images: 670,828 Image Size (GB):96.1
	ACRIN 6677	Modalities: MR,CT Number of Images: 717,070 Image Size (GB):86.9

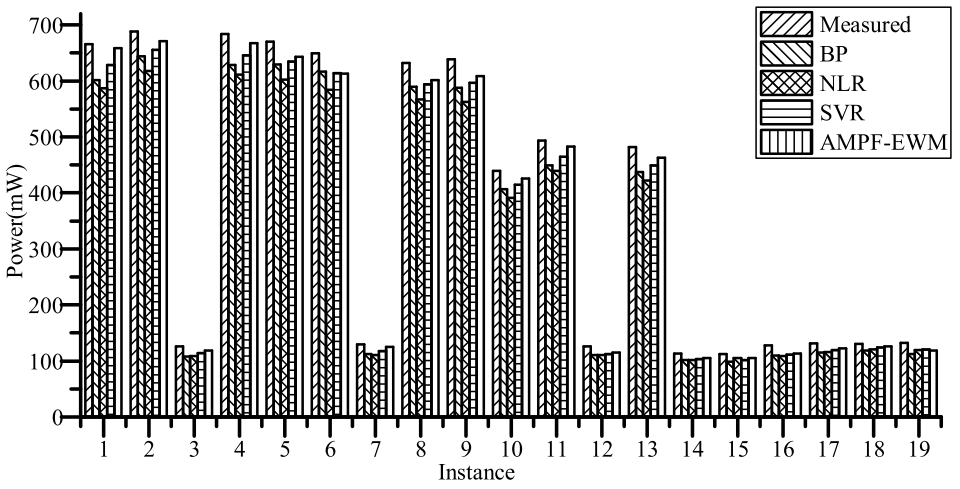

Figure 4. Comparison of AMPF with actual measured power and prediction of existing methods.

we can see that all the used methods can fit the curve well, but the curves fitted by the three methods still have errors. Above errors to predict the power of medical images will make big error.

Figure 4 shows the predicted power comparison among the AMPF realized by EWM and each single predictors of 19 instances selected in the random test set. The abscissa represents the instance number, the ordinate represents the power, and the Measured, BP, NLR, SVR, and AMPF-EWM in the legend respectively indicates measured power, power predicted by BP, power predicted by NLR, power predicted by SVR, and the power predicted by AMPF with EWM. In the figure, we can see that AMPF realized by EWM shows good prediction ability. Even in 6, 15, and 19 instances, AMPF realized by EWM is not worse among each predictors. From the figure, the AMPF realized by EWM model has the advantage compared with the single predictors.

Table II shows the performance comparison among each prediction model mentioned by Eq. (6) and Eq. (8) corresponding to Fig. 4. Among each model, the *RMSE*,

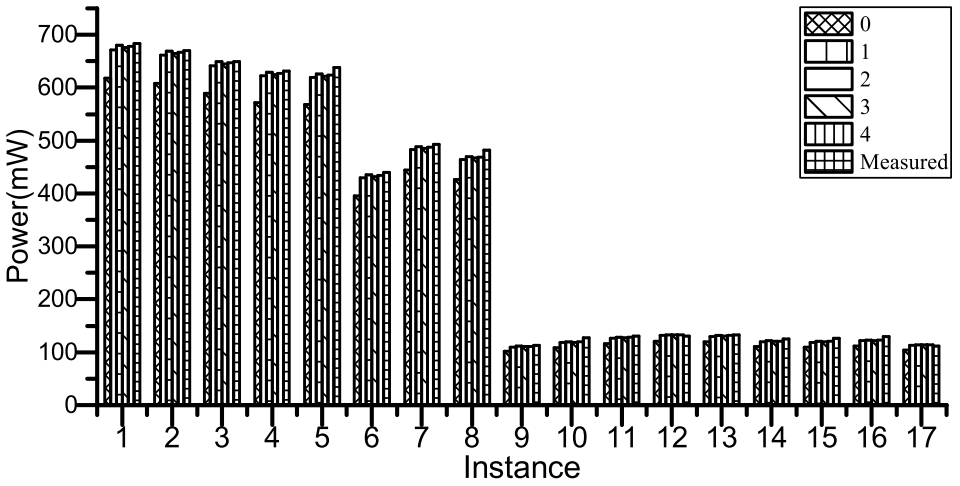

Figure 5. Comparison between measured and predicted value of AMPF under different weak models.

Table II. Performance comparison of various methods.

	RMSE	MAPE	RRMSE	MAE	SSE	R^2	Accuracy
BP	42.3710	0.0828	0.0860	39.9482	21543.6061	0.9549	0.9145
SVR	60.9155	0.1125	0.1134	57.3733	44528.3206	0.9069	0.8874
NLR	32.0704	0.0652	0.0686	30.7208	12342.1153	0.9742	0.9332
AMPF-EWM	17.4545	0.0354	0.0389	16.4367	3655.9	0.9919	0.9646

Table III. Performance comparison of AMPF under different weak prediction models.

	RMSE	MAPE	RRMSE	MAE	SSE	R^2	Accuracy
0 predictor	60.9155	0.1125	0.1134	57.3733	44528.3206	0.9069	0.8958
1 predictor	12.3701	0.0257	0.0306	11.338	1836.26	0.9961	0.9788
2 predictors	6.6560	0.0135	0.021	5.0231	531.6311	0.9988	0.9786
3 predictors	17.4545	0.0354	0.0389	16.4367	3655.9	0.9919	0.9646
4 predictors	8.0996	0.0169	0.0236	6.8398	787.2548	0.9983	0.9798

MAPE, *RRMSE*, *MAE*, and *SSE* of the AMPF realized by EWM model have smaller value than those of BP, SVR, and NLR models. The R^2 of AMPF with EWM model has a bigger value than that of BP, SVR, and NLR models. For accuracy, AMPF with EWM model also has the biggest among each predictors. This shows AMPF with EWM model has better accuracy. This also shows AMPF method proposed in this paper is effective.

Figure 5 shows the comparison between the measured power and the predicted value of AMPF realized by EWM under the different number of weak prediction models. The abscissa represents the number of the prediction instance, the ordinate represents the power, and the number in the legend indicates the number of weak predictors. From the figure, we can see that the prediction value of any combination of weak prediction models is better than that of a single weak predictor. In combining 1, 2, 3 or 4 weak predictors, they are closer to the measured value. Table III shows the performance comparison between them. The AMPF combining two weak predictors yields the highest R^2. The performance of AMPF combining two predictors on *RMSE, MAPE, RRMSE, MAE,* and *SSE* is also better than that of combining one, three, and four predictors. For accuracy, AMPF having four weak predictors with 0.9798 has the best accuracy among other models, followed by AMPF having one weak and two weak predictors with 0.9788 and 0.9786. The accuracy of AMPF having three weak predictors with 0.9646 is the last but one, and the accuracy of AMPF having zero weak predictors with 0.8958 is the last.

Figure 6 shows the prediction comparison between AMPF implemented by EWM and AdaBoost of 17 instances selected in the random test set. In the figure, the abscissa represents the number of prediction examples, and the ordinate represents the power, and the AMPF-EWM, AMPF -AdaBoost in the legend respectively indicates AMPF realized by EWM and AMPF realized by AdaBoost. It can be seen from the figure that the predicted value of AMPF realized by EWM and AdaBoost approaches the real measured value, showing good prediction ability. Table IV shows the performance comparison under three weak predictors for them. The R^2 of AMPF implemented by EWM reaches 0.9919, and that of AMPF implemented by AdaBoost reaches 0.9989. Numerical results show that both the AMPF implemented by EWM and the AMPF implemented by AdaBoost have good goodness of fit, and later is better than the former in goodness of fit. For *RMSE*, *MAPE*, *RRMSE*, *MAE*, *SSE*, and accuracy, the AMPF implemented by AdaBoost is also better than that implemented by EWM.

Major portion of time consumed by the proposed method is in training, and the time consumed for prediction after training is almost the same. Therefore, this paper indicates the time consumed by training. Figure 7 shows the comparison of training time for AMPF implemented by EWM and AdaBoost methods. The abscissa in the

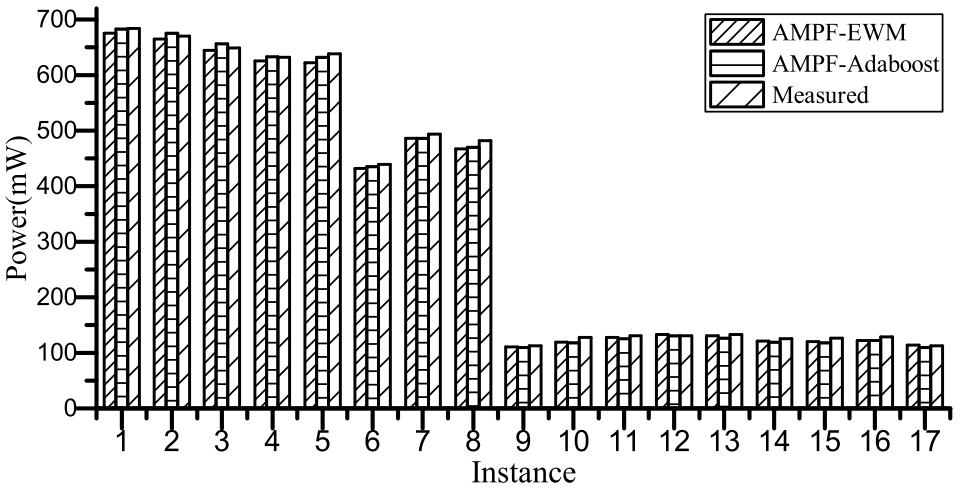

Figure 6. Prediction Comparison of AMPF realized by different methods.

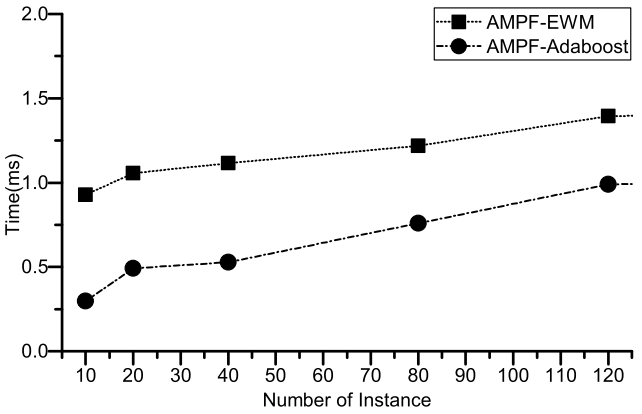

Figure 7. Time comparison of AMPF realized by different methods.

Table IV. Performance comparison of AMPF realized by different methods.

	RMSE	MAPE	RRMSE	MAE	SSE	R^2	Accuracy
EWM-AMPF	17.4545	0.0354	0.0389	16.4367	3655.9	0.9919	0.9646
AdaBoost-AMPF	6.6268	0.0170	0.0257	5.9007	526.9884	0.9989	0.9828

figure represents the number of training sets, and the ordinate represents the training time, and the AMPF-EWM, AMPF-AdaBoost in the legend respectively indicates AMPF realized by EWM and AMPF realized by AdaBoost. It can be seen from the figure that as the number of training instances increases, the time of AMPF implemented by EWM and AdaBoost methods consumed also increases. The training time of AMPF implemented by EWM is more than that of AMPF implemented by AdaBoost under the same training set. For the consumed time, when the number of training sets is less than 100, the time consumed by AMPF implemented by EWM is twice that of the AMPF implemented by AdaBoost. However, when the training set is greater than 100, the time consumed by AMPF implemented by EWM is about 1.3 times that of the AMPF implemented by AdaBoost.

5. CONCLUSION

Accurately predicting the power of the medical image is an important issue. Using a single predictor can predict the power value of the medical image, but lacks accuracy. Therefore, we propose an AMPF framework to solve this problem. It makes use of the two strong prediction methods and is realized in three steps. The experimental results show the effectiveness, feasibility, and good performance of AMPF. Through the above experiments, we conclude the following.

(1) The medical image power model based on the AMPF model can improve the prediction accuracy.
(2) The performance of each combined weak predictor method used to realize AMPF is not very different, but the time used in the training has some differences.
(3) As an approach tool, the AMPF method also has broad application prospects in the fields requiring accurate prediction, such as disease prediction, power load prediction, and so forth.

ACKNOWLEDGMENT

This work was supported in part by the National Natural Science Foundation of China under Grant No. 61862051; the Science and Technology Foundation of Guizhou Province under Grant No. [2019]1447; the Philosophy and Social Science Planning Youth Project of Guizhou Province under Grant No. 18GZQN36; the Top-notch Talent Program of Guizhou province under Grant No. KY[2018]080; the Nature Science Foundation of Educational Department under Grant Nos. [2022]094 and [2022]100; the Nature Science Foundation of Qiannan Normal University for Nationalities under Grant Nos. 2020qnsyzd03, QNSY2018JS013, QNSYRC201714, QNSYRC201715. We also acknowledge group of embedded real-time systems for their effective advice and constructive suggestions.

REFERENCES

[1] E. H. Houssein, M. M. Emam, A. A. Ali, and P. N. Suganthan, "Deep and machine learning techniques for medical imaging-based breast cancer: A comprehensive review," Expert Syst. Appl. **167**, 114161 (2021).

[2] H. Naeem and A. A. Bin-Salem, "A CNN-LSTM network with multi-level feature extraction-based approach for automated detection of coronavirus from CT scan and X-ray images," Applied Soft Computing **113**, 107918 (2021).

[3] S. Shaees, H. Naeem, M. Arslan, M. R. Naeem, S. H. Ali, and H. Aldabbas, "Facial emotion recognition using transfer learning," *IEEE Int'l. Conf. on Computing and Information Technology, (ICCIT-1441)* (IEEE, Piscataway, NJ, 2020), pp. 1–5.

[4] H. Naeem, F. Ullah, M. R. Naeem, S. Khalid, D. Vasan, S. Jabbar, and S. Saeed, "Malware detection in industrial internet of things based on image visualization and deep learning," Ad Hoc Networks **105**, 102154 (2020).

[5] M. H. M. Lu, M. Hack, R. Hewitt, M. S. Weaver, and J. J. Brown, "Power consumption and temperature increase in large area active-matrix OLED displays," J. Display Technology **4**, 47–53 (2008).

[6] A. Carroll and G. Heiser, "An analysis of power consumption in a smartphone," *In 2010 USENIX Annual Technical Conf. (USENIX ATC 10)* (USENIX Association, Berkeley, CA, 2010).

[7] X. Chen, Y. Chen, Z. Ma, and F. C. Fernandes, "How is energy consumed in smartphone display applications?," *Proc. 14th Workshop on Mobile Computing Systems and Applications* (ACM, New York, NY, 2013).

[8] A. Pathak, Y. C. Hu, and M. Zhang, "Where is the energy spent inside my app? Fine grained energy accounting on smartphones with eprof," *Proc. 7th ACM European Conf. on Computer Systems* (ACM, New York, NY, 2012), pp. 29–42.

[9] M. Dong and L. Zhong, "Power modeling and optimization for OLED displays," IEEE Trans. Mobile Computing **11**, 1587–1599 (2012).

[10] P. K. Choubey, A. K. Singh, R. B. Bankapur, P. C. SB Vaisakh, and B. Manoj Prabhu, "Content aware targeted image manipulation to reduce power consumption in OLED panels," *Proc. 8th Int'l. Conf. on Contemporary Computing (IC3)* (IEEE, Piscataway, NJ,, 2015), pp. 467–471.

[11] M. Hort, M. Kechagia, F. Sarro, and M. Harman, "A survey of performance optimization for mobile applications," IEEE Trans. Softw. Eng. (2021).

[12] L. T. Duan, B Guo, Y. Shen, Y. Wang, W. L. Zhang, and W. Xiong, "A low power OLED method based on HSV color space," Optoelectronics Laser **24**, 1878–1883 (2013).

[13] D. G. Li, B. Guo, R. L. Zhang, Y. Z. Ma, Z. Q. Ren, X. G. Zhao, Q. Tan, and J. K. Li, "Multi-region power consumption optimization of AMOLED display based on visual saliency," J. Softw. **31**, 2741–2755 (2020).

[14] S. Asnani, M. G. Canu, L. Farinetti, and B. Montrucchio, "On producing energy-efficient and contrast-enhanced images for OLED-based mobile devices," Pervasive and Mobile Computing **2021**, 101384.

[15] A. B. Dalton and C. S.. Ellis, "Sensing user intention and context for energy management," *9th Workshop on Hot Topics in Operating Systems (HotOS IX)* (USENIX Association, Berkeley, CA, 2003), pp. 151–156.

[16] S. H. Na, W. K. Min, D. H. Kim, H. W. Hwang, Y. M. Ha, and H. J. Kim, "Enhancement of picture quality on ultra-low brightness by optimizing the electrical potential required for OLED charging in the AMOLED displays," J. Inf. Disp. **22**, 275 (2021).

[17] L. Zhou, M. Xu, X. H. Xia, J. H. Zou, L. R. Zhang, D. X. Luo, W. J. Wu, L. Wang, and J. B. Peng, "Power consumption model for AMOLED display panel based on 2T-1C pixel circuit," J. Display Technology **12**, 1064–1069 (2016).

[18] S. G. Lim, K. Lee, and Y. J. Kim, "Mobile AMOLED display power model considering I–R drop in smartphones," IEEE Trans. Industrial Electronics **68**, 2694–2702 (2020).

[19] M. Dong, Y. S. K. Choi, and L.. Zhong, "Power modeling of graphical user interfaces on OLED displays," *2009 46th ACM/IEEE Design Automation Conf.* (IEEE, Piscataway, NJ, 2009), pp. 652–657.

[20] J. H. Park and Y. J. Kim, "Accurate power model for mobile AMOLED displays," Electron. Lett. **51**, 553–555 (2015).

[21] D. Kim, W. Jung, and H. Cha, "Runtime power estimation of mobile AMOLED displays," *Proc. Design, Automation & Test in Europe Conf. & Exhibition (DATE 2013)* (IEEE, Piscataway, NJ, 2013), pp. 61–64.

[22] C. Kim, S. Hong, K. Lee, and Y. J. Kim, "High-accurate and fast power model based on channel dependency for mobile AMOLED displays," IEEE Access **6**, 73380–73394 (2018).

[23] S. Hong, S. W. Kim, and Y. J. Kim, "3 channel dependency-based power model for mobile AMOLED displays," *2017 54th ACM/EDAC/IEEE Design Automation Conf. (DAC)* (IEEE, Piscataway, NJ, 2017), pp. 1–6.

[24] P. Dash and Y. C. Hu, "How much battery does dark mode save? An accurate OLED display power profiler for modern smartphones," *Proc. 19th Annual Int'l. Conf. on Mobile Systems, Applications, and Services* (ACM, New York, NY, 2021), 2021, pp. 323–335.

[25] https://wiki.cancerimagingarchive.net/display/Public/Collections.